# Evaluation of PFC2D Grain-Based Model for simulation of confinement-dependent rock strength degradation and failure processes

**Conference Paper** · January 2011

CITATIONS
25

READS
550

**4 authors**, including:

Navid Bahrani
Dalhousie University
**40** PUBLICATIONS **483** CITATIONS
SEE PROFILE

Benoît Valley
Université de Neuchâtel
**120** PUBLICATIONS **1,641** CITATIONS
SEE PROFILE

P. K. Kaiser
Laurentian University
**217** PUBLICATIONS **10,121** CITATIONS
SEE PROFILE

ARMA 11-156

# Evaluation of PFC2D Grain-Based Model for Simulation of Confinement-Dependent Rock Strength Degradation and Failure Processes

Bahrani, N. and Valley, B.
*Geomechanics Research Centre, MIRARCO – Mining Innovation, Sudbury, ON, Canada*
Kaiser, P.K.
*CEMI – Centre for Excellence in Mining Innovation, Sudbury, ON, Canada*
Pierce, M.
*Itasca Consulting Group, Inc., Minneapolis, MN, USA*



This paper was prepared for presentation at the 45th US Rock Mechanics / Geomechanics Symposium held in San Francisco, CA, June 26–29, 2011.



**ABSTRACT:** Estimation of rock mass strength has become more critical in recent years due to the increase in the number of mining and civil projects at greater depths (> 2 km). Empirical approaches for the estimation of rock mass strength (e.g., Hoek-Brown/GSI) are primarily based on experiences at shallow depths and low confinement problems (e.g., tunnel wall failure), and therefore may not be representative for the strength in highly confined rock masses (e.g., for the core of pillars or abutments at depth). In this study an attempt is made to investigate the strength of rock masses, using the discrete element code PFC2D. For this purpose, the recently developed PFC2D Grain-Based Model (GBM) was used to match the laboratory response of intact and granulated Wombeyan marble. The term "granulated" refers to a heat treated sample where the grains have been completely separated at their boundaries due to anisotropy and contrast of their thermo-elastic properties. This material is considered to represent an analogue for a randomly jointed rock mass. It is shown that the PFC2D-GBM calibrated to unconfined and confined intact marble strengths and then to the unconfined granulated marble strength, underestimates the strength of the confined granulated marble. This problem was resolved by increasing the grain boundary friction angle in the granulated model to account for micro-scale roughness of the grain boundaries as observed in the microscopic image of the granulated marble. The calibration methodology taken to obtain micro-properties for both intact and granulated marble as well as implications for the determination of rock mass strength at various confinement levels are discussed.

## 1. INTRODUCTION

With the increase in the number of mining and civil projects at great depths (>2 km), the validity of common empirical approaches calibrated at shallow depths needs to be evaluated. Moreover, at such depths due to high ratios of excavation-induced stress to rock mass strength, a number of challenges arise and therefore a better estimation of rock mass strength is critical for the safe and efficient development of underground infra-structures such as tunnels and pillars.

Conventional approaches for the determination of rock mass strength (e.g., Hoek-Brown failure criterion [1] with the GSI classification system [2, 3]) have been primarily established based on experiences from tunnels at relatively shallow to moderate depths, and observations near excavations where confinement is relatively low (in the 5 to 10 MPa range). Therefore, the application of these techniques for the estimation of confined rock mass strength, relevant for the design of wide pillars, could be flawed and may lead to costly design errors.

In this study, the discrete element code, PFC2D [4] was used to investigate the strength of rock masses by calibrating the models to laboratory test results of undamaged and damaged samples. The damaged samples are considered to represent an analogue for a randomly jointed rock mass.

Different methods in PFC2D for modeling brittle failing rocks are first briefly reviewed. The PFC2D grain-based model (GBM) is then used to match the laboratory response of the intact and granulated Wombeyan marble reported by Gerogiannopoulos [5]. The calibration process to choose the GBM micro-properties as well as the transition in the failure modes with increasing confinement captured by the GBM is explained in detail. Finally, implications of the test and modeling results for confinement-dependent rock mass strength degradation are discussed.

## 2. MODELING BRITTLE FAILING ROCKS IN PFC2D

The Discrete Element Method (DEM) is increasingly used by researchers in the field of geomechanics. One of the applications of DEM is the simulation of intact rocks and rock masses by considering the rock as an assemblage of circular or spherical particles, cemented at their contact points. This method, which is called the Bonded Particle Model (BPM), has been implemented in two- and three-dimensional codes such as PFC2D [4] and PFC3D [6].

The main advantage of the BPM over conventional continuum codes is that pre-defined complex empirical constitutive relations are replaced with simpler particle contact logic without requiring plasticity rules [7]. Cracking in this method is explicitly simulated as bond breakage. Once a bond breaks, the displacement field as well as transition to the residual strength are controlled by particle geometry and friction at particle-particle contacts. This explicitly captures a fundamental characteristic of brittle failing rocks known as cohesion weakening/frictional strengthening [8, 9]. The concept of cohesion weakening/frictional strengthening for brittle rocks was captured in the damage-controlled tests combined with the Griffith locus theory by Martin and Chandler [8] who showed that with increasing damage the cohesional strength component is gradually lost and the frictional strength component mobilizes.

One of the applications of BPM is the micro-mechanical modeling of cracking and simulation of brittle rock failure processes. Several approaches have been proposed in this regard including the conventional bonded particle model, the clustered particle model, the clumped particle model and the grain-based model. These are briefly reviewed next.

### *2.1. Conventional Bonded Particle Model (CBPM)*

The conventional bonded particle model (referred to as CBPM here) is based on the assumption that rock consists of circular or spherical particles bonded together at their contact points. The particles and bonds can then be considered as rock grains and grain boundaries, respectively. Contact and parallel bonds are the two basic bond models in PFC. A contact bond behaves as glue between two particles, connecting them at their contact point. A parallel bond acts as an additional cement-like material deposited over a finite area (a cylinder) between the two particles. Cho et al. [10] suggested that the parallel bond model as opposed to the contact bond model is a more realistic option for simulating rocks since the bond breakage results in stiffness reduction.

In the CBPM, the calibration of micro-contact parameters is usually performed on the uniaxial compressive strength (UCS). Diederichs [11] showed that the CBPM calibration to UCS significantly over-predicts the tensile strength of rock and the failure envelope is linear (Figure 1). This implies that calibration of the CBPM to the tensile strength will underestimate the rock's UCS.

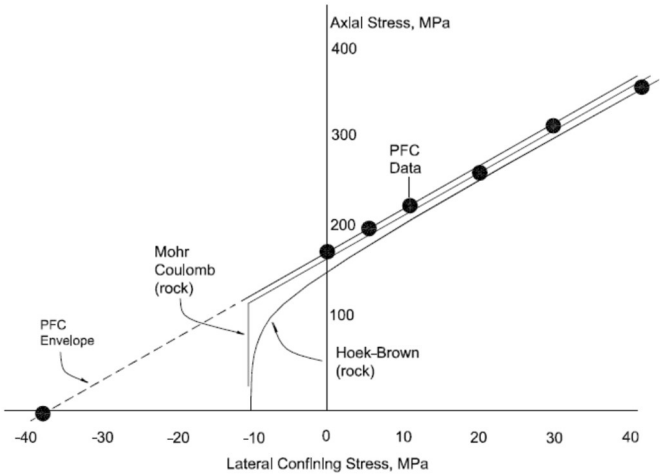


Figure 1 Linear failure envelope and overestimation of tensile strength in CBPM when calibrated to UCS [11].

Potyondy and Cundall [7] established the hypothesis that this limitation is due to the lack of interlocking between the circular or spherical particles forming the CBPM which does not reflect the highly interlocked fabric of crystalline rocks.

### *2.2. Clustered Particle Model (ClsPM)*

Potyondy and Cundall [7] introduced an algorithm in PFC2D which generates particle clusters of complex interlocking shapes (called the clustered particle model and referred to as ClsPM here). The size of the clusters is defined by the maximum number of particles in a cluster. The insert in Figure 2 shows an example of ClsPM with 7 particles inside the clusters.

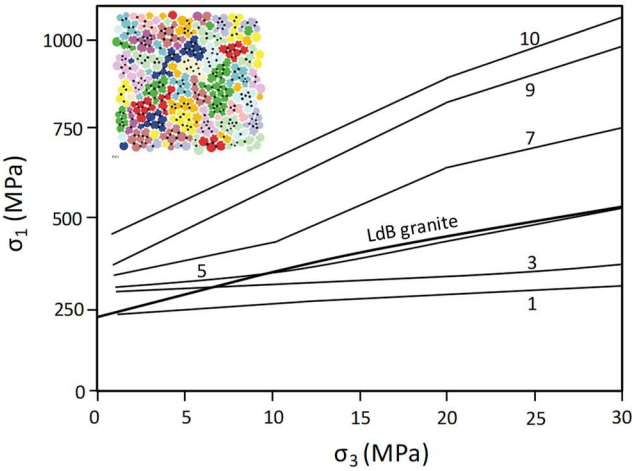


Figure 2 Clustered particle model representing irregular-shaped grains and the effect of cluster size on the strength envelope for unbreakable clusters (after Potyondy and Cundall [7]); note: the numbers with each envelope represent the number of particles in a cluster (i.e., the cluster size).

Potyondy and Cundall [7] used unbreakable clusters which force the cracks to occur along cluster boundaries, and showed that the UCS and the slope of the strength envelope exceeded those of Lac du Bonnet (LdB) granite when the number of particles inside the clusters increases from 1 to 10 as shown in Figure 2.

Cho et al. [10] performed a sensitivity analysis on the cluster size in an unbreakable ClsPM and found that $\sigma_t$/UCS decreases to about 0.1 for a cluster size of 14 from 0.3 for a cluster size of 1 (ClsPM with a cluster size of 1 corresponds to the CBPM). The strength ratio of 0.1 is still too high compared to the measured $\sigma_t$/UCS $\leq$ 0.05 for LdB granite. Such unrealistically high strength ratios led them to use an alternative approach called the clumped particle model in which the clusters are rigid.

### 2.3. *Clumped Particle Model (ClmPM)*

A clump consists of more than one particle but moves as a single rigid object. This differs from a cluster, in which the internal contacts between particles are retained, resulting in a deformable grain. The irregular shape of a rock grain can be captured more realistically with clumps since very large contact overlaps between the circular particles can be used to generate the clump.

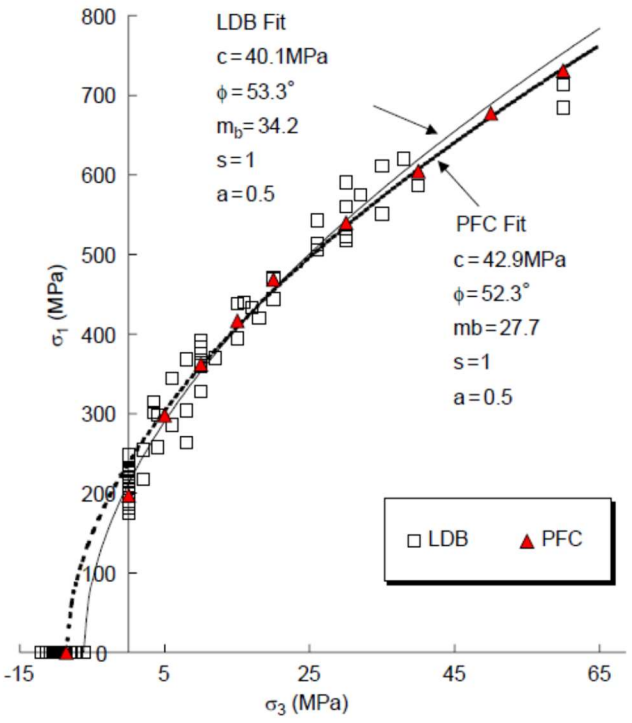


Figure 3 Failure envelope predicted by ClpPM showed excellent agreement with that of LdB granite [10].

Cho et al. [10] used the clumped particle model (referred to as ClmPM here) and were able to overcome the limitations of CBPM and ClsPM mentioned earlier. They showed that dilation significantly increased with increasing clump size, however the strength ratio ($\sigma_t$/UCS) remained close to 0.07, similar to that of a crystalline rock. Moreover, they found excellent agreement between the failure envelope predicted by the ClmPM and that of the LdB granite, as illustrated by Figure 3.

### 2.4. *Grain-Based Model (GBM)*

The Grain-Based Model (GBM) developed by Potyondy [12, 13] provides a synthetic material with deformable, breakable polygonal grains, cemented at their adjoining sides. Grains in this approach mimic a cemented granular material and the interface (grain boundaries) mimics a cemented joint. The advantage of PFC2D-GBM over UDEC-GBM [14, 15] is the ability to simulate both unbreakable and breakable grains. The grains in UDEC-GBM are assumed to be unbreakable which may not be realistic since intra-grain fractures are most likely to happen in compression [16], particularly at high confining pressures.

The PFC2D-GBM is created by 1) generating a grain structure, and 2) overlaying the grain structure on a bonded particle model, called the base material. At each grain interface, the parallel bonds are replaced by the smooth joint contacts. When the smooth joint is created, the contact model and parallel bond, if present, are deleted and replaced by the smooth joint contact. The properties of the smooth joint, except for the dip angle and dip direction, are then inherited from the contact and the two contacting entities. It is also possible to assign the smooth joint properties directly to the model.

Potyondy [12] used the unbreakable grains in the PFC2D-GBM and was able to match the laboratory response of Äspö diorite subjected to direct tension, unconfined and confined (with 7 MPa confinement) compressive tests. The model showed very good agreement in the crack initiation and propagation levels, modulus and the failure modes with the laboratory test results of Äspö diorite.

## 3. GRAIN-BASED MODELS OF WOMBEYAN MARBLE

In this study, the PFC2D-GBM was calibrated to the laboratory response of intact and granulated coarse-grained Wombeyan marble [5], with an average grain size of 1 to 2 mm. The purpose of this analysis is four-fold:

- systematically evaluate PFC2D-GBM for simulating brittle failing rocks, according to strength ratio ($\sigma_t$/UCS), friction angle and nonlinear failure envelope;
- assess the PFC2D-GBM's ability in capturing the transition in the failure mode from axial splitting at low confinement to shear failure at high confinement;

- investigate the capability of the PFC2D-GBM to simulate the confinement dependent strength degradation of a damaged rock; and
- assess implications for rock mass behavior by considering the damaged marble as an analogue of a randomly jointed rock mass.

### *3.1. Intact versus Granulated Wombeyan Marble*

The laboratory behavior of the coarse-grained Wombeyan marble has been studied by Paterson [17], Rosengren and Jaeger [18] and Gerogiannopoulos [5]. The confinement in the laboratory tests performed by Paterson [17] ranged from 0 to 100 MPa. He observed a transition in the failure mode from axial fracturing to a well-defined, single shear band formation at low confinement (i.e., 3.5 MPa), to conjugate shear banding at higher confinement (i.e., 35 MPa), to ductile behavior at extremely high confining pressure (i.e., 100 MPa). The confinement level in the tests performed by Rosengren and Jaeger [18] and Gerogiannopoulos [5] was ~35 MPa.

Rosengren and Jaeger [18] and Gerogiannopoulos [5] found that if the coarse-grained Wombeyan marble is heated to ~600°C, the anisotropy of thermal expansion of calcite causes complete separation of the grains at their boundaries. Rosengren and Jaeger [18] mentioned that during heating, the sample initially emitted a continuous 'pinging' sound, probably caused by tensile failure of the grain boundaries. This was confirmed by microscopic examination of this material which showed that the grain boundaries have been opened up (Figure 4), and the very low tensile strength of 0.03 MPa, measured in a direct tension test with failure occurring by fracturing along the grain boundaries. This material, referred to as "granulated" marble, with randomly oriented grain boundaries can be considered as an analogue for a randomly jointed rock mass.

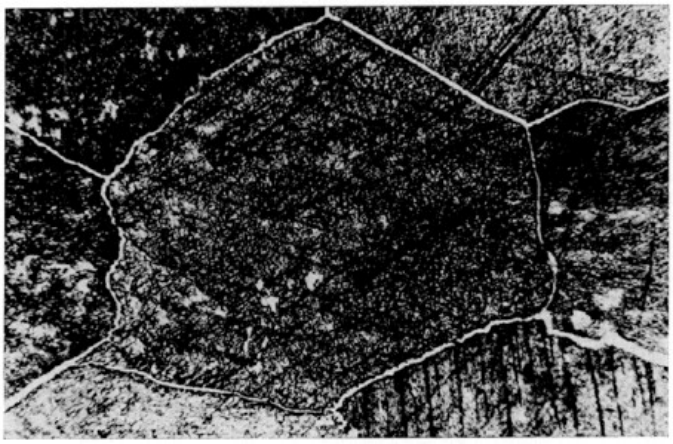

Figure 4 Open grain boundaries (in white) in granulated Wombeyan marble [18]. Width of field is 2.4 mm.

As illustrated in Figure 5, heating the marble reduced its uniaxial compressive strength to less than half of its intact UCS. A small amount of confinement, however, rapidly increased the confined strength, with an equivalent friction (including dilation) angle of 65° at low confinement as was also reported by Rosengren and Jaeger [18]. For confining pressures greater than 10 MPa, the strength increases to about 80% of the marble's intact strength and the friction angle decreases to ~40° between 5 and 15 MPa, and ~20° above 15 MPa.

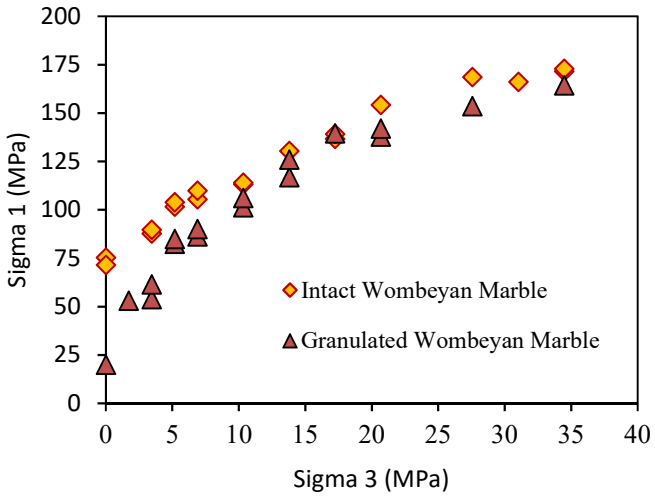


Figure 5 Triaxial test results of intact and granulated coarse-grained Wombeyan marble reported by Gerogiannopoulos [5].

### *3.2. Model Generation*

A small, 20 by 50 mm sample was generated to match the laboratory response of both intact and granulated Wombeyan marble under varying confining pressures. The GBM is therefore smaller than the actual samples reported by Gerogiannopoulos [5]. This was required to reduce the calculation time. According to Potyondy and Cundall [7], however, scale effects are not significant when modeling rocks in compressive loading conditions provided the particle size is relatively small compared to the size of the model.

The average grain size of Wombeyan marble according to Gerogiannopoulos [5] and Rosengren and Jaeger [18] is between 1 and 2 mm. A simplified grain structure (Figure 6a) containing two different-sized equally and randomly distributed polygonal grains with average grain size of 1 and 2 mm was generated according to the procedure described by Potyondy [19].

The ratio of sample height to sample diameter (H/D = 2.5), as well as the ratio of largest grain diameter to sample diameter ($d_{Gmax}$/D = 0.1) used in the simulations are in agreement with those suggested by ISRM [20]. Each grain is made of multiple particles from the base material with a maximum diameter, $d_{max}$, of 0.40 mm (shown in Figure 6b). This is smaller than the minimum grain size ($d_{Gmin}$ = 1 mm) in the model.

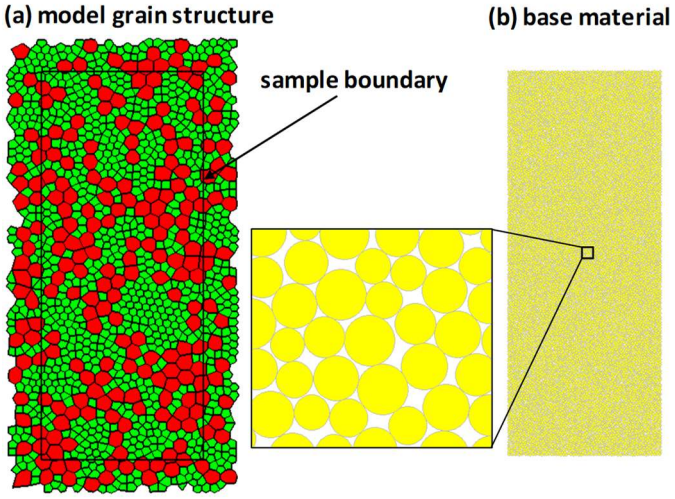


Figure 6 a) grain structure consists of two different-sized equally distributed polygonal grains. Green and red polygons are grains with diameters of 1 and 2 mm, respectively; b) base material consists of particles with minimum particle size (diameter) of 0.4 mm. Note that sample width and height are 2 and 5 cm, respectively.

Using the algorithm described by Potyondy [13], the grain structure (Figure 6a) was overlaid on the base material (Figure 6b), and then contacts along the grain interfaces were replaced by smooth joint contacts. Figure 7 shows the grain-based model which consists of smooth joint contacts (grain boundaries) and particles cemented together (grains).

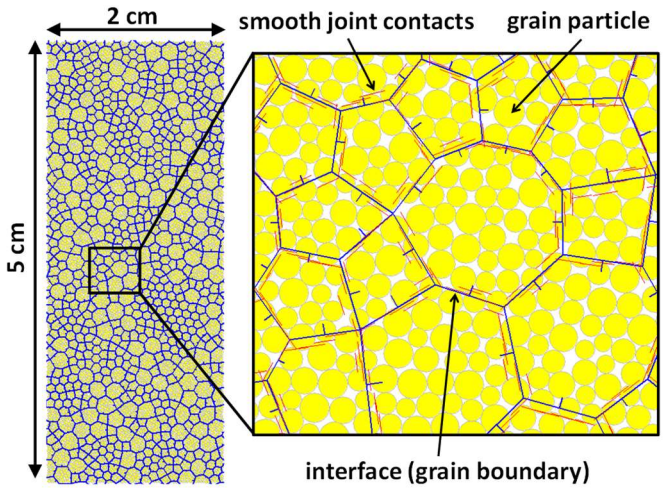


Figure 7 Grain-based model constructed by overlaying the grain structure on the base material and replacing the interfaces with the smooth joint contacts.

### *3.3. Calibration Procedure*

An extensive calibration with breakable grains in the GBM was carried out to match laboratory test results of both intact and granulated marble. The calibration was performed based on the assumption that heating intact marble samples only affected the mechanical properties of the grain boundaries but not the grains. Therefore, once the micro-properties of the intact marble in the GBM were determined, the behavior of granulated marble is captured by only changing the micro-properties of the smooth joint contacts representing the grain boundaries. The calibration process is summarized in four steps:

1. Calibration on intact marble tensile and uniaxial compressive strengths: The model was first calibrated to the modulus, as well as the tensile and compressive strengths of intact marble. It was found that the material tensile strength was correlated to the smooth joint tensile strength. For the compressive strength, the smooth joint cohesion and friction angle (grain boundary properties) as well as the parallel bond tensile strength, cohesion and friction angle (grain properties) were adjusted. The Young's modulus was found to depend on the smooth joint, parallel bond and particle contact (both grain and grain boundaries) stiffness values.

2. Calibration on intact marble confined strength: Triaxial test simulations were then carried out with the parameters obtained from step one. The micro-properties of both grain and grain boundaries affect the friction angle and therefore the triaxial strength.

   Once changes in these parameters were made to capture the intact marble confined strength, step one was repeated to ensure model calibration with respect to E, $\sigma_t$ and UCS of intact marble (first loop). This loop was repeated until an acceptable agreement between the GBM modulus, tensile, unconfined and confined strengths and those of intact Wombeyan marble were found.

3. Calibration on granulated marble tensile and uniaxial compressive strengths: For the granulated marble, as mentioned earlier, only micro-properties of the smooth joint contacts, representing the grain boundaries, were changed. For this purpose, the smooth joint contact stiffness parameters, tensile strength and cohesion were reduced.

   If a match with the properties of the granulated marble (E, $\sigma_t$ and UCS) was not achieved, calibration had to be redone from step one (second loop).

4. Calibration on granulated marble confined strength: The model which was previously calibrated on granulated marble E, $\sigma_t$ and UCS, was then tested for its confined strength. It was observed that this model significantly underestimates the confined strength of the granulated marble (low friction angle). The friction angle of the smooth joints therefore had to be increased. This resulted in an increase in the UCS of the granulated marble. Therefore step 3 had to be redone to make sure that the model E, $\sigma_t$ and UCS agreed with those of granulated marble (third loop).

It should be noted that the adopted calibration procedure is an iterative approach whereby, at each step, the number of trials to achieve an acceptable macro-property (e.g., material tensile strength) was kept to a manageable number by choosing a key micro-property (e.g., smooth joint tensile strength). As mentioned above, the calibration was performed with a large number of parameters, including tensile, unconfined and confined strength as well as modulus of both the intact and granulated marble. Due to the large number of micro-properties included in the PFC2D-GBM and despite the number of imposed constraints explained above, the system is indeterminate. Hence, multiple combinations of micro-properties can lead to a well calibrated but not unique model. The solution presented here represents such a model that is qualitatively equivalent to other possible solutions. This lack of uniqueness, however, is not seen as a deficiency as combinations of different material parameters in nature can lead to similar behaviors in terms of failure mechanisms and thus strength.

### *3.4. Grain-Based Model Results*

Table 1 summarizes the micro-properties of the grain in the intact and granulated GBM of Wombeyan marble obtained through this calibration process. As shown in this table, the grains in both intact and granulated models were assigned the same micro-properties, based on the assumption that heating the intact marble did not affect the mechanical properties of the grains. Only changes in the smooth joint properties, representing the grain boundaries, were required to simulate the transition from intact to granulated marble.

Table 1 Grain (particle and parallel bond) micro-properties for intact and granulated marble.

| Properties | Intact and Granulated marble |
|---|---|
| $R_{min}$ | 0.12 mm |
| $R_{max}/R_{min}$ | 1.66 |
| $k_n/k_s$ and $\bar{k}^n/\bar{k}^s$ | 2.5 |
| $E_c$ and $\bar{E}_c$ | 60.0 GPa |
| $\mu$ | 0.5 |
| $\bar{\lambda}$ | 1 |
| $\bar{\sigma}_c$ | 150 MPa |
| $\bar{C}$ | 300 MPa |
| $\bar{\phi}$ | 40° |

$R_{min}$ is the minimum particle radius and $R_{max}/R_{min}$ is the ratio of maximum to minimum particles radii. $k_n/k_s$ and $\bar{k}^n/\bar{k}^s$ are the contact and parallel bond stiffness ratios (normal to shear). $E_c$ and $\bar{E}_c$ are the contact and parallel bond moduli, respectively. $\bar{\lambda}$ is the parallel bond radius multiplier. μ is the particle friction coefficient. $\bar{\sigma}_c$, $\bar{C}$, and $\bar{\phi}$ are the parallel bond tensile strength, cohesion, and friction angle, respectively. Table 2 lists the smooth joint contact properties for intact and granulated GBM of Wombeyan marble.

Table 2 Grain boundary (smooth joint contact) micro-properties for intact and granulated marble.

| Properties | Intact marble | Granulated marble |
|---|---|---|
| $\bar{k}_n$ and $\bar{k}_s$ | 0.6 × inherited | 0.023 × inherited |
| $\sigma_b$ | 5 MPa | 0.1 MPa |
| $C_b$ | 50 MPa | 0.5 MPa |
| $\phi_b$ | 35° | 75° |

$\bar{k}_n$ and $\bar{k}_s$ are the smooth joint contact normal and shear stiffnesses, respectively, and $\sigma_b$, $C_b$ and $\phi_b$ are the smooth joint tensile strength, cohesion and friction angle. Once the smooth joint is created, its stiffness properties are inherited from the contact and the two contacting particles, according to the following equations:

$$\bar{k}_n = (k_n/A) + \bar{k}^n$$

$$\bar{k}_s = (k_s/A) + \bar{k}^s$$

$$A = 2\bar{R}t, \;\; t = 1$$

where $A$ is the cross sectional area of the smooth joint, $t$ is the disk (particle) thickness, $\bar{R}$ is the smooth joint contact radius (i.e., half length of smooth joint contact) which is derived from $R^A$ and $R^B$, the two particle radii, from the following relation:

$$\bar{R} = \bar{\lambda}\min(R^A, R^B)$$

As mentioned earlier, heating the intact marble resulted in a complete separation of the grains at their boundaries and a correspondingly low tensile strength of 0.03 MPa. Such a low tensile strength was obtained by lowering the smooth joint contact tensile strength to the low value of 0.1 MPa in the granulated model, from that of 5.0 MPa in the intact model. The UCS of the granulated model was calibrated by reducing the smooth joint cohesion from that of 50.0 MPa in the intact model to 0.5 MPa.

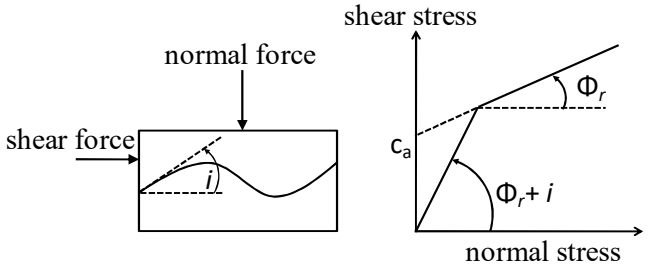


Figure 8 Bilinear strength envelope of a rough surface in direct shear test from Patton [21], and surface roughness model illustrating the roughness angle *i*.

The key point in this calibration was the increase in the smooth joint contact "friction angle" from 35° in the intact model to 75° in the granulated model. Such a high angle for the grain boundaries in the granulated model may seem unrealistic. But if it is understood that it contains a friction and dilation component, as explained by the Patton [21] bilinear strength envelope of a rough

discontinuity in a direct shear test (Figure 8), it is more realistic. The adopted "friction plus dilation" angle of 75°, is close to the angle of 65° reported by Rosengren and Jaeger [18], who fitted a Mohr-Coulomb envelope to the low confinement range of the granulated Wombeyan marble.

At low confinement, failure occurs by sliding along the inclined rough surface with a friction angle of $\phi_r + i$, where $\phi_r$ is the residual friction angle and $i$ is the inclination or roughness angle of the inclined surface. Once the confinement is increased above some critical value, the sliding on the inclined asperity surfaces is inhibited, and the shear strength is then defined by the residual friction angle and apparent cohesion ($c_a$) of the intact rock making up asperities between sliding joints. Such a rough surface can be seen along the grain boundaries in the microscopic image of the granulated marble in Figure 4.

In the GBM, the grain boundaries are modeled to be smooth surfaces using the smooth joint contact logic, and therefore the roughness of the asperities is not explicitly simulated. The behavior of the granulated marble at low confinement had then to be replicated by increasing the "friction" of the smooth joints from the "residual" friction angle ($\phi_r$) of 35° in the intact model plus a dilational component of 40° to arrive at an "apparent friction" angle ($\phi_r + i$) of 75° in the granulated model. For a rock mass or a grain assembly as in the damaged marble, a bulking process (an overall volume increase due to grain rearrangement, potentially some grain rotation, leading to the opening of grain boundaries) occurs as the fabric is disrupted. This process leads to an equivalent behavior as described by Patton [21] for joints and by Dusseault and Morgenstern [22] for locked sands.

Table 3 shows that the tensile and uniaxial strengths of both intact and granulated Wombeyan marble are very well captured by the GBM. The Young's modulus of intact marble is also very close to the measured modulus. The GBM, however, slightly overestimates the modulus of granulated marble. Considering the 97.5 % reduction in the laboratory measured modulus from intact to granulated marble, the 86.7 % reduction captured by the GBM is considered to be acceptable.

Table 3 Comparison between laboratory test results and PFC simulation of intact and granulated Wombeyan marble. Tensile strength of intact and granulated Wombeyan marble were obtained from Mahmutoglu [23], and Rosengren and Jaeger [18], respectively.

| Properties | Intact marble | | Granulated marble | |
|---|---|---|---|---|
| | Lab test | GBM | Lab test | GBM |
| UCS (MPa) | 73.5 | 68.4 | 20.0 | 21.9 |
| E (GPa) | 67.2 | 64.0 | 1.7 | 8.5 |
| $\sigma_t$ (MPa) | 3.4 | 3.4 | 0.03 | 0.07 |
| $\sigma_t$ /UCS | 0.046 | 0.050 | 0.002 | 0.003 |

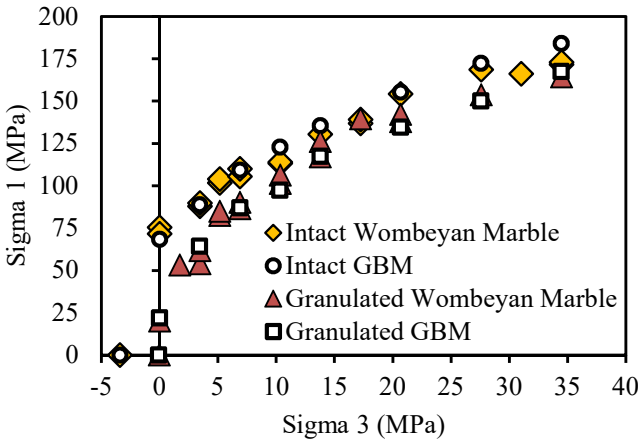


Figure 9 Comparison of tensile, uniaxial and triaxial strengths measured in the laboratory with results obtained by PFC2D-GBM for intact and granulated Wombeyan marble.

Figure 9 compares the Wombeyan marble tests results including tensile, uniaxial and triaxial strengths, with those obtained from numerical simulation. This figure suggests that the correct tensile to compressive strength ratio, reasonable friction angle as well as the non-linear failure envelope can be well captured by the PFC2D-GBM.

### *3.5. Macroscopic Response*

The confinement dependent failure modes of Wombeyan marble in the tests performed by Paterson [17] are shown in Figure 10. Similar failure modes were predicted by PFC2D-GBM. Figure 11 shows the location, orientation and nature of both inter- and intra-grain cracking (tensile or shear) in the direct tension and uniaxial compression tests, as well as the triaxial tests with 3.5 and 35 MPa confining pressures.

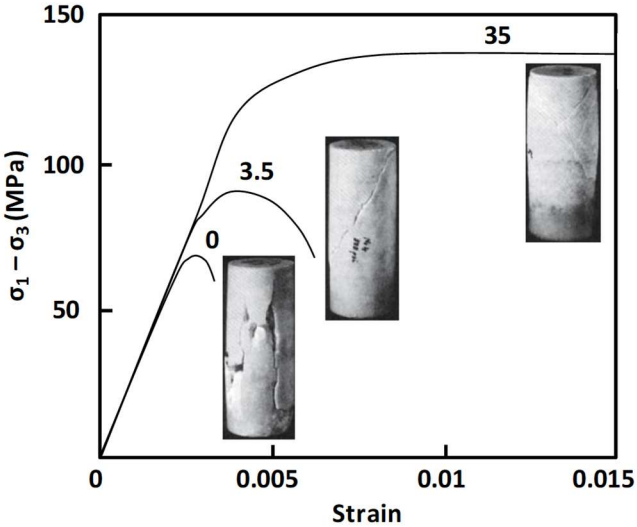


Figure 10 Stress-strain curves and transition in the failure mode of intact Wombeyan marble from axial splitting to shear failure (from Paterson [17]). Numbers refer to confining pressures in MPa.

Sub-horizontal inter-grain tensile cracks define the failure mode in the direct tension test (Figure 11a). This

agrees with laboratory studies by Mosher et al. [16] who found that inter-grain fractures dominate tensile failure in brittle rocks. In the uniaxial compression test as shown in Figure 11b, the cracks are oriented approximately parallel to the axial load. Most of the fractures are inter-grain tension cracks. At some locations in the sample, the interaction of the sub-vertical cracks resulted in a macroscopic axial fracture which is consistent with the failure mode of Wombeyan marble at zero confinement shown in Figure 10.

In the confined compression tests, the interaction between inter- and intra-grain cracks have formed macroscopic shear bands (Figure 11c and Figure 11d), which is consistent with macroscopic shear failure shown in Figure 10. This is more pronounced at higher confinement. For example, two major shear bands have developed in the case of the 35 MPa confinement test, with several intra-grain tensile failures. Note that Figure 11 shows all of the cracks that formed from the beginning of the test to 50%, 80% and 90% of the peak strength in the post-peak region in the direct tension, unconfined and confined compression tests, respectively.

## 4. IMPLICATIONS FOR CONFINEMENT-DEPENDENT ROCK MASS STRENGTH DEGRADATION

Advanced numerical codes such as PFC used in this study are still too complex for standard engineering and thus rarely used by practitioners. As a practical alternative to anticipate rock behavior, continuum models are used but this brings the challenge of selecting appropriate equivalent continuum properties for naturally discontinuous rock masses. Rock mass classification systems, such as the GSI (see below), are used to obtain parameters for empirical failure criteria such as the Hoek-Brown failure criterion.

The generalized Hoek-Brown failure criterion (first equation in [1]) is commonly used to estimate the equivalent continuum rock mass strength from the intact rock strength measured in the laboratory, using the Geological Strength Index (GSI) chart introduced by Hoek [2] and constants, $C_m$ and $C_s$ to degrade the intact strength to the rock mass strength. The GSI system provides a means for rating the quality of a rock mass based on rock block geometry as well as joint surface condition [2, 3 & 24]. The constants $C_m$ and $C_s$ take the values of 28 and 9, respectively, and affect the Hoek-Brown parameters $m_b$ and $s$ through the following relations:

$$m_b = m_i exp\left(\frac{GSI - 100}{C_m}\right)$$

$$s = exp\left(\frac{GSI - 100}{C_s}\right)$$

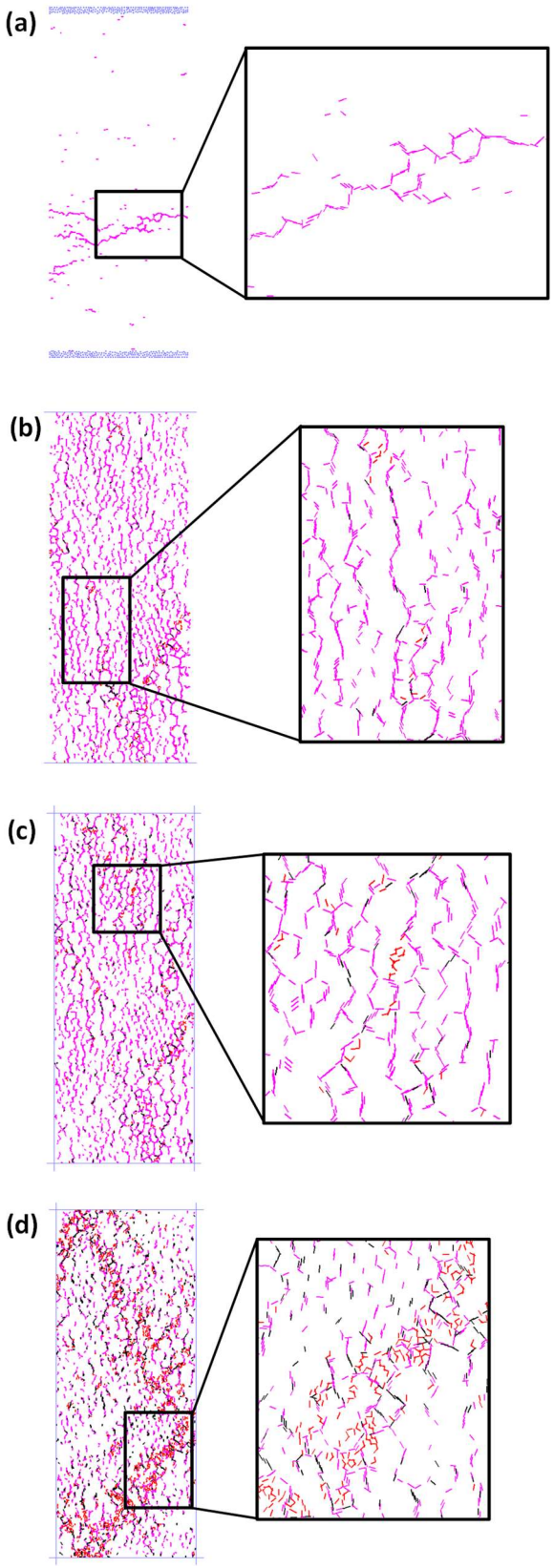


Figure 11 Failure modes of intact marble predicted by PFC2D-GBM in: a) direct tension test; b) uniaxial compressive test; c) and d) triaxial tests with 3.5 and 35 MPa confining pressures, respectively. In this figure pink and black refer to inter-grain tensile and shear cracks, respectively, and red and blue refer to intra-grain tensile and shear cracks.

The validity of these empirically determined constants under confinement conditions is the core of this investigation. For this purpose, the response of the thermally damaged marble presented and modeled above is used as an analogue for a randomly jointed rock mass to evaluate the validity of these factors. However for such a rock mass analogue, the interlocking rock mass characteristics, including block size and joint condition [24], and therefore the GSI rating, cannot be explicitly evaluated.

An alternate approach to relate damaged sample properties with rock mass interlocking is to determine an equivalent GSI value under unconfined conditions. As presented in Figure 12, the damaged marble unconfined compressive strength reduces to about 25% of the intact marble strength (UCS = 74 MPa, $m_i = 6.6$), which correspond to a GSI of about 75. One can then compare the confined strength predicted by the GSI system with the measured strength. For confinement levels exceeding 0.1UCS, the GSI system significantly underestimates the strength (grey arrow on Figure 12). At these confinement levels, the damaged marble or "rock mass" strength is about 90% of the intact rock conditions with an equivalent GSI of about 97.

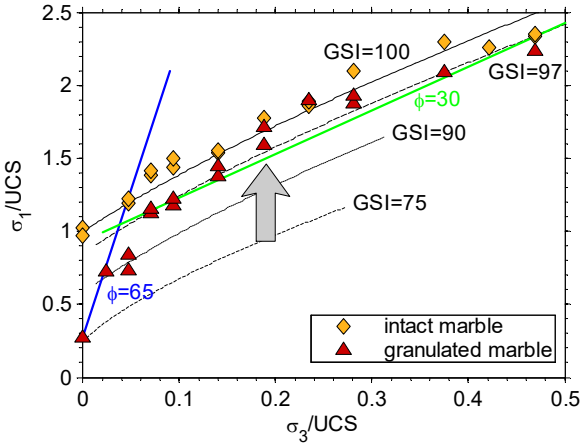


Figure 12 Interpretation of granulated (damaged) Wombeyan marble strength data as an analogue for randomly jointed rock masses.

The results presented here suggest that the GSI approach could underestimate the confined strength of rock masses behave like the damaged marble with a transition from a tensile to a single shear to a conjugate shear failure mode. In other words, the results suggest that there is a much greater degradation of the *s*-value at low confinement than at high confinement. The degradation constant $C_s$ described above, must then be much higher than 9 in the confined range (>0.08UCS) [25].

By analogue with Patton's approach presented above, the damaged marble, and by extension a corresponding brittle rock mass would have $s = 0.062$, for the unconfined state, and an apparent $s_a = 0.717$ for the confined state at >0.08UCS corresponding to a GSI ~ 97.

Alternatively, with a constant GSI equal to 75 throughout the confinement range, equivalent to the standard GSI approach, the $C_s$-value will need to be confinement dependent. It should increase from $C_s = 9$ in unconfined condition to $C_s$~80 at higher confinement (i.e., $\sigma_3 > 0.08$UCS).

The conclusions derived in this paper are valid for rock masses with rough joints and tight blocky fabrics with irregular block geometries, where confinement will strongly interlock the joints and prevent fabric disruption, forcing intact rock failure through asperities at block boundaries or through blocks (grains). This is supported by the equivalent friction angles reported by Rosengren and Jaeger [18] (see Figure 12); at low confinement an equivalent friction of 65° is observed suggesting asperities overriding ($\phi_r + i$) and rock mass bulking with block fabric disruption and possibly rotation (see Section 3.4), while under confined conditions the equivalent friction angle is similar to that of intact rock (about 30° on average for $\sigma_3$ between 0.1 and 0.5UCS).

Rock masses rated with a GSI of 75 spans a broad range of conditions, with block size ranging from 0.3 to 1.5 m or more [26] and joint conditions from very good (very rough) to fair (smooth and moderately weathered). The micro-photograph of the damaged marble (Figure 4) shows that grain boundaries are very rough and that the structure is highly interlocked (an element that is not considered in the GSI system).

This suggests that the GBM results and interpretation presented above are valid for rock masses for which strength degradation of grain or block boundaries and disruption of interlocked grain or rock block dominate the behavior. In such cases, a significant strength increase is to be anticipated at the transition from a grain boundary and shape controlled dilational behavior at low confinement, to a shear failure controlled behavior with an apparent cohesion (or elevated *s*-value) for the confined rock mass strength.

However, the applicability of the results presented here (i.e., a significantly higher confined strength for rock masses than predicted by the GSI approach) to rock masses with other characteristics, (e.g., rock masses with larger block size, poorer joint conditions and less interlocking) is the subject of current research. The insight gained by the current GBM results, showing the importance of joint roughness and fabric disruption to reproduce the laboratory results obtained on damage marbles, suggest that the strength increase under confined conditions (grey arrow on Figure 12) could be less pronounced for rock mass with relatively poor joint conditions, relatively loose block assemblies (allowing easy block rotation), and with relatively weak intact rock.

## 5. CONCLUSIONS

The determination of rock mass strength is critical at any stage of mining and civil projects. The increase in the number of projects at great depths generates a number of challenges in the development of the underground infrastructures such as tunnels and pillars. Conventional approaches to characterize rock mass strength such as the GSI classification system have primarily been established from the data related to tunnels at shallow to moderate depths and from observations near excavation walls. Therefore, the application of these techniques for estimating rock mass strength (for example the strength in a pillar core) could be flawed.

The grain-based model in PFC2D was used to capture the laboratory response of intact and granulated marble [5] to investigate the strength of rock masses at various confinement levels. The term "granulated" refers to a heat treated sample where the grain boundaries have been seperated . Such a material is considered here to represent an analogue for a randomly jointed rock mass.

After an extensive calibration effort based on the approach explained in Section 3.3, the PFC2D grain-based model proved to have the capability of reproducing many fundamental characteristics of brittle failing rocks including true tensile to compressive strength ratio, non-linear failure envelope, reasonable friction angle, as well as the change in the failure mode from axial splitting at low confinement to shear failure at higher confinement. The simulation results suggest that the strength of samples (either intact or granulated) at low confinement, is mainly driven by the failure of grain boundaries (tensile or shear), whereas the interaction between inter- and intra-grain cracks and grain or block fabric drives the failure of confined samples.

The results described in this paper have implications for the modeling of highly confined rock masses using the advanced numerical codes such as PFC2D, PFC3D and ELFEN [27]. The discontinuous nature of rock masses in these codes is simulated by assigning the discontinuities explicitly to the models using a tool known as Discrete Fracture Network (DFN) simulation. A DFN allows for the detailed consideration of the rock mass joint fabric including discontinuity geometry (length and orientation), and persistence at the adopted scale. The rough nature of the discontinuities and the related dilatant characteristics are usually ignored in these simulations. Therefore calibration of numerical models to low confinement problems (e.g., tunnel wall instability) tends to underestimate the strength of highly confined rock masses such as pillar cores and abutments at great depths.

The results described in this paper also have implications for the estimation of highly confined rock masses using empirical methods such as the GSI system. Whereas the GSI system is well-calibrated and proven to be helpful for the engineering of support in tunnels and caverns, the findings in this paper suggest that the resulting confined strength may be significantly underestimated for moderately jointed, hard rock masses.

## LIST OF SYMBOLS

| | |
|---|---|
| DEM | Discrete Element Method |
| PFC2D | Particle Flow Code in two dimensions |
| PFC3D | Particle Flow Code in three dimensions |
| UDEC | Universal Distinct Element Code |
| BPM | Bonded Particle Model |
| CBPM | Conventional Bonded Particle Model |
| ClsPM | Clustered Particle Model |
| ClmPM | Clumped Particle Model |
| GBM | Grain-Based Model |
| DFN | Discrete Fracture Network |
| LdB | Lac du Bonnet |
| H | Sample/model height |
| D | Sample/model diameter |
| $d_{Gmax}$ | Maximum grain diameter (size) |
| $d_{Gmin}$ | Minimum grain diameter (size) |
| $d_{max}$ | Maximum particle diameter (size) |
| $R_{max}$ | Maximum particle radius |
| $R_{min}$ | Minimum particle radius |
| $t$ | Disk (particle) thickness |
| $k_n$ | Contact normal stiffness |
| $k_s$ | Contact shear stiffness |
| $E_c$ | Contact modulus |
| μ | Particle friction coefficient |
| $\bar{k}^n$ | Parallel bond normal stiffness |
| $\bar{k}^s$ | Parallel bond shear stiffness |
| $\bar{E}_c$ | Parallel bond modulus |
| $\bar{\sigma}_c$ | Parallel bond tensile strength |
| $\bar{C}$ | Parallel bond cohesion |
| $\bar{\phi}$ | Parallel bond friction angle |
| $\bar{\lambda}$ | Parallel bond radius multiplier |
| $\bar{k}_n$ | Smooth joint normal stiffness |
| $\bar{k}_s$ | Smooth joint shear stiffness |
| $\sigma_b$ | Smooth joint tensile strength |
| $C_b$ | Smooth joint cohesion |
| $\phi_b$ | Smooth joint friction angle |
| $A$ | Smooth joint cross sectional area |
| $\bar{R}$ | Smooth joint radius |
| $C_a$ | Apparent cohesion |
| $\phi_r$ | Residual friction angle |
| $i$ | Roughness angle |
| UCS | Uniaxial Compressive Strength |
| $\sigma_{ci}$ | Uniaxial compressive strength of intact rock |
| $\sigma_t$ | Tensile strength |
| E | Modulus |
| GSI | Geological Strength Index |
| $m_b$ | Hoek-Brown "slope" constant for rock mass |
| $m_i$ | Hoek-Brown "slope" constant for intact rock |
| $s$ | Hoek-Brown constant ($s$ = 1 for intact rock) |

$s_a$ Apparent $s$
$C_m$ Hoek-Brown degradation constant ($C_m = 28$)
$C_s$ Hoek-Brown degradation constant ($C_s = 9$)


## AKNOWLEDGMENTS

This research project is supported by Rio Tinto, Natural Sciences and Engineering Research Council of Canada (NSERC) and Itasca Consulting Group through its Itasca Education Partnership (IEP) program. The authors would like to thank Drs. Ted Brown and Evert Hoek for providing the marble laboratory test data and Professor Derek Martin for the discussion at the early stage of the manuscript preparation. Special thanks to Dr. David Potyondy and conference reviewers for reviewing the paper and their constructive comments. The first author would also like to acknowledge Drs. Matthew Pierce, David Potyondy, Sacha Emam and Xavier Garcia from Itasca Consulting Group for their help with the modeling.


## REFERENCES


1. Hoek, E. and E. T. Brown (1997). Practical estimates of rock mass strength. *Int. J. Rock Mech. Min. Sci.*, 34 (8): 1165-1186.
2. Hoek E. 1994. Strength of rock and rock masses. *ISRM News J.*, 2(2): 4-16.
3. Hoek E., Kaiser P.K. and Bawden W.F. 1995. *Rock Support for Underground Excavations in Hard Rock*. Rotterdom, NE: Balkema, 215p.
4. Itasca Consulting Group, Inc. 2008a. Particle Flow Code in 2 dimensions (PFC2D), Ver. 4.0. Minneapolis.
5. Gerogiannopoulos N.G. 1976. A critical state approach to rock mechanics. PhD thesis, University of London, 325p.
6. Itasca Consulting Group, Inc. 2008b. Particle Flow Code in 3 dimensions (PFC3D), Ver. 4.0. Minneapolis.
7. Potyondy D.O. and Cundall P.A. 2004. A bonded particle model for rock. *Int. J. Rock Mech. Min. Sci.*, 41: 1329-1364.
8. Martin C.D. and Chandler N.A. 1994. The progressive fracture of Lac du Bonnet granite. *Int. J. Rock Mech. Min. Sci. & Geomech. Abstr.*, 31 (6): 643-659.
9. Hajiabdolmajid, V., Kaiser, P. K., and Martin, C. D., 2002. Modelling brittle failure of rock. *Int. J. Rock Mech. Min. Sci.*, 39 (6): 731-741.
10. Cho N., Martin C.D. and Sego D.C. 2007. A clumped particle model for rock. *Int. J. Rock Mech. Min. Sci.*, 44: 997-1007.
11. Diederichs. M. 2000. Instablity of hard rock masses; the role of tensile damage and relaxation, PhD thesis, University of Waterloo. 617 p.
12. Potyondy D.O. 2010. A grain-based model for rock: approaching the true microstructure. In: *Proc. Rock Mech. in the Nordic Countries*, 10p.
13. Potyondy D. 2010. PFC2D grain-based models. Itasca Consulting Group, Inc. Technical Memorandum ICG6773-L, May 28, 2010.
14. Lan H., Martin C.D. and Hu B. 2010. Effect of heterogeneity of brittle rock on micromechanical extensile behavior during compression loading. *J. Geophys. Res.*, 115: B01202.
15. Kazerani T. and Zhao J. 2010. Micromechanical parameters in bonded particle model for modeling of brittle material failure, *Int. J. Numer. Anal. Meth. Geomech.*, 34: 1877-1895.
16. Mosher S., Berger R.L. and Anderson D.E. 1975. Fracture characteristics of two granites. *Rock Mech.*, 7: 167-176.
17. Paterson M.S. 1958. Experimental deformation and faulting in Wombeyan marble. *Geol. Soc. America. Bull.*, 69: 465-476.
18. Rosengren K.J., Jaeger J.C. 1968. The mechanical properties of an interlocked low-porosity aggregate. *Géotechnique*, 18: 317-326.
19. Potyondy D. 2010. PFC2D grain-structure generator. Itasca Consulting Group, Inc. Technical Memorandum ICG6772-L, May 28, 2010.
20. Bieniawski Z.T. and Bernede M.J. 1979. Suggested methods for determining the uniaxial compressive strength and deformability of rock materials. *Int. J. Rock Mech. Min. Sci. & Geomech. Abstract*,16(2): 138-140.
21. Patton, F.D. 1966. Multiple mode of shear failure in rock. *1st Int. Conf. on Rock Mech.*, Lisbon, 509-511.
22. Dusseault M.B. and Morgenstern N.R. 1979. Locked sands. *Q. J. Eng. Geol.*, 12: 117-131.
23. Mahmutoglu Y. 1998. Mechanical Behaviour of cyclically heated fine grained rock. *Rock Mech. Rock Engng.*, 31:169-179.
24. Cai, M., Kaiser, P. K., 2006. Visualization of rock mass classification systems. *Geotech. Geol. Eng.*, 24 (4), 1089-1102.
25. Kaiser, P. K. and B.H. Kim**,** 2008. Rock mechanics advances of underground construction and mining. Keynote lecture, *Korea Rock Mech. Symp*, Seoul, 1-16.
26. Cai, M., Kaiser, P. K., Tasaka, Y., Minami, M., 2007. Determination of residual strength parameters of jointed rock masses using the GSI system. *Int. J. Rock Mech. Min. Sci.,*44 (2): 247-265.
27. Rockfield, 2007. ELFEN. Rockfield technology Ltd., Swansea, UK: http://www.rockfield.co.uk